



CHORUS

This is the accepted manuscript made available via CHORUS. The article has been published as:

Chiral gauge field and axial anomaly in a Weyl semimetal

Chao-Xing Liu, Peng Ye, and Xiao-Liang Qi

Phys. Rev. B **87**, 235306 — Published 10 June 2013

DOI: [10.1103/PhysRevB.87.235306](https://doi.org/10.1103/PhysRevB.87.235306)

Chiral gauge field and axial anomaly in a Weyl semi-metal

Chao-Xing Liu¹, Peng Ye^{2,3} and Xiao-Liang Qi⁴

¹ *Department of Physics, The Pennsylvania State University, University Park, Pennsylvania 16802-6300*

² *Perimeter Institute for Theoretical Physics, Waterloo, Ontario, Canada N2L 2Y5*

³ *Institute for Advanced Study, Tsinghua University, Beijing, 100084, People's Republic of China*

⁴ *Department of Physics, McCullough Building, Stanford University, Stanford, CA 94305-4045*

(Dated: May 21, 2013)

Weyl fermions are two-component chiral fermions in (3+1)-dimensions. When coupled to a gauge field, the Weyl fermion is known to have an axial anomaly, which means the current conservation of the left-handed and right-handed Weyl fermions cannot be preserved separately. Recently, Weyl fermions have been proposed in condensed matter systems named as “Weyl semi-metals”. In this paper we propose a Weyl semi-metal phase in magnetically doped topological insulators, and study the axial anomaly in this system. We propose that the magnetic fluctuation in this system plays the role of a “chiral gauge field” which minimally couples to the Weyl fermions with opposite charges for two chiralities. We study the anomaly equation of this system and discuss its physical consequences, including one-dimensional chiral modes in a ferromagnetic vortex line, and a novel plasmon-magnon coupling.

PACS numbers: 71.90.+q, 73.43.-f, 03.65.Vf, 75.50.Pp

I. INTRODUCTION

In the quantum field theory, a (3+1)-dimensional massless Dirac fermion is decomposed to two independent two-component fermions known as the Weyl fermions. Weyl fermion has a definite chirality, lefthanded or righthanded, determined by the sign of its spin polarization along the momentum direction.¹ Classically, the lefthanded and righthanded Weyl fermions are decoupled and can be coupled independently to two gauge fields, leading to a separate charge conservation. The gauge field that couples differently to Weyl fermions with two chiralities is called a chiral gauge field. For example the SU(2) gauge field in the Standard Model is a chiral gauge field. It is well-known that the chiral charge conservation is violated in a quantum theory of Weyl fermions in a background gauge field, which is known as the axial anomaly²⁻⁴.

Recently, Weyl fermions are also introduced into condensed matter physics. The Weyl fermions are shown to be the topologically robust boundary states of (4+1)-d time-reversal (TR) invariant topological insulators (TI)⁵, and the axial anomaly corresponds to a topological response of the (4+1)-d TI. This approach is related to the domain wall fermion approach⁶ and Callan-Harvey effect⁷ in high energy physics. By dimensional reduction, the (4+1)-d topological insulator is reduced to the (3+1)-d TI⁸⁻¹⁰ and the Weyl fermion is reduced to (2+1)-d surface states of the TI. Weyl fermions also appear directly in (3+1)-d gapless electron systems, which are named as “Weyl semi-metals”^{4,11-21}. Since a system with both TR and parity (P) symmetries have all energy bands doubly degenerate, the Weyl semi-metal state can only be realized in a system breaking TR and/or P symmetry.

A natural question is whether the chiral gauge field can be realized in the Weyl semi-metals, and if yes, what is the physical consequence. In this paper, we address

these questions in TR breaking Weyl semi-metals. We show that generically a ferromagnetic moment couples to the Weyl fermions as a chiral gauge field. As an explicit example system, we study a model of magnetically doped topological insulator, which can be driven into the Weyl semi-metal phase with strong enough magnetic moments. The presence of the chiral gauge field leads to an anomaly equation satisfied by the charge current, which results in new topological phenomena such as chiral one-dimensional states in a magnetic vortex, and a topological coupling between spin fluctuation and plasmons.

II. CHIRAL GAUGE FIELD AND ANOMALY EQUATION

We start with a general discussion of Weyl fermions in condensed matter physics. In a weakly interacting crystalline material, Weyl fermion states generically appear when two energy bands cross at a generic point \vec{K}_0 in the Brillouin zone. The low energy physics around \vec{K}_0 is described by a two-component Hamiltonian $h(\mathbf{k}) = \hbar \sum_{i,j=x,y,z} v_{ij} k_i \sigma_j$, with k_i the momentum away from \vec{K}_0 , and σ_j the Pauli matrices. The matrix v_{ij} describes the generic linear coupling between momentum and spin degree of freedom described by σ_j . By rotating the basis one can always diagonalize v_{ij} , and the three diagonal components are anisotropic velocities. Without losing generality, we restrict our discussion on isotropic Weyl fermions with the simple Hamiltonian $h(\mathbf{k}) = \hbar v_f \vec{\sigma} \cdot \vec{k}$. Our results on anomaly and chiral gauge field is insensitive to the anisotropy in the velocity. The sign of the Fermi velocity v_f determines the chirality of Weyl fermion.

According to the Nielsen-Ninomiya theorem^{22,23}, in a lattice model the number of Weyl fermions with opposite chiralities must be equal. Consequently, the mini-

minimum number of Weyl fermions in a Brillouin zone is 2. Moreover, because TR symmetry preserves the chirality of Weyl fermion, in TR invariant system the minimum number of Weyl fermions is 4¹⁵. In the following, we focus on the “minimal Weyl semi-metal” which break TR but preserves P, with two Weyl fermions of opposite chiralities at wavevectors \vec{K}_0 and $-\vec{K}_0$, related to each other by spatial inversion.

We consider an arbitrary perturbation to the system of two Weyl fermions. As long as the perturbation is so smooth that the momentum transfer is much smaller than $2|\vec{K}_0|$, the two Weyl fermions remain decoupled. The perturbed Hamiltonian can be generally written in the second quantized form as $H_L = \int d^3r \psi_L^\dagger(\mathbf{r}) [\hbar v_f \vec{\sigma} \cdot (-i\vec{\nabla})] \psi_L(\mathbf{r}) + \delta H_L$, with the two-component spinor field operator $\psi_L(\mathbf{r})$ annihilating the lefthanded Weyl fermions. The perturbation Hamiltonian δH_L has a gradient expansion $\delta H_L = \int d^3r \psi_L^\dagger(\mathbf{r}) [\hbar v_f \vec{\sigma} \cdot \vec{a}_L(\mathbf{r}) + a_{0L}(\mathbf{r}) + O(-i\vec{\nabla})] \psi_L(\mathbf{r})$, where the higher order terms containing one or more space-time derivatives has been omitted, which are marginal or irrelevant in long wavelength limit and does not affect our discussion below.

The field $a_{\mu L} = (a_{0L}, \vec{a}_L)$ behaves as a gauge field with smooth spatial and temporal dependence. Similarly one can define the gauge field $a_{\mu R}$ minimally coupled to the righthanded Weyl fermions with the Hamiltonian $H_R = \int d^3r \psi_R^\dagger(\mathbf{r}) [-\hbar v_f (-i\vec{\nabla} + \vec{a}_R(\mathbf{r})) \cdot \vec{\sigma} + a_{0R}(\mathbf{r})] \psi_R(\mathbf{r})$. (We would like to note that similar idea has been successfully applied to graphene where strain field acts as a gauge field^{24,25}.) Writing the two Weyl fermions into a 4-component Dirac fermion, and including the minimal coupling to electromagnetic field A_μ , we obtain

$$H = \int d^3r \psi^\dagger(\mathbf{r}) \left[\hbar v_f \left((-i\vec{\nabla} + \vec{A}(\mathbf{r})) \cdot \vec{\sigma} \tau_z + \vec{a}(\mathbf{r}) \cdot \vec{\sigma} \right) + a_0(\mathbf{r}) \tau_z + \tilde{A}_0(\mathbf{r}) \right] \psi(\mathbf{r}) \quad (1)$$

with $\psi^\dagger(\mathbf{r}) = (\psi_L^\dagger(\mathbf{r}), \psi_R^\dagger(\mathbf{r}))$, $\tilde{A}_\mu = A_\mu + (a_{\mu L} + a_{\mu R})/2$ and $a_\mu = (a_{\mu L} - a_{\mu R})/2$. We see that $a_{\mu L} + a_{\mu R}$ contributes a correction to the electromagnetic field, while $a_{\mu L} - a_{\mu R}$ has different P and TR properties as A_μ , and acts as a chiral gauge field. In the following, we will consider the perturbation induced by a ferromagnetic moment fluctuation, which only contributes to \vec{a} since it is TR odd and P even. Therefore we will take $\tilde{A}_\mu = A_\mu$ in the rest of the paper.

As is known from quantum field theory, a Weyl fermion coupled to a gauge field has an axial anomaly, which means the classical charge conservation symmetry is broken in the full quantum theory^{1,26,27}. The anomaly is described by the anomaly equation $\partial_\mu j^{\mu L(R)} = (-) \frac{1}{32\pi^2} \epsilon^{\lambda\rho\mu\nu} f_{\lambda\rho}^{L(R)} f_{\mu\nu}^{L(R)}$ where $f_{\mu\nu}^{L(R)} = \partial_\mu a_{\nu L(R)} - \partial_\nu a_{\mu L(R)}$. Using the field strength $F_{\mu\nu} = \partial_\mu A_\nu - \partial_\nu A_\mu$ and $f_{\mu\nu} = \partial_\mu a_\nu - \partial_\nu a_\mu$, and the charge current $j^\mu = j^{\mu L} + j^{\mu R}$ and the axial current $j^{\mu 5} = j^{\mu L} - j^{\mu R}$, the

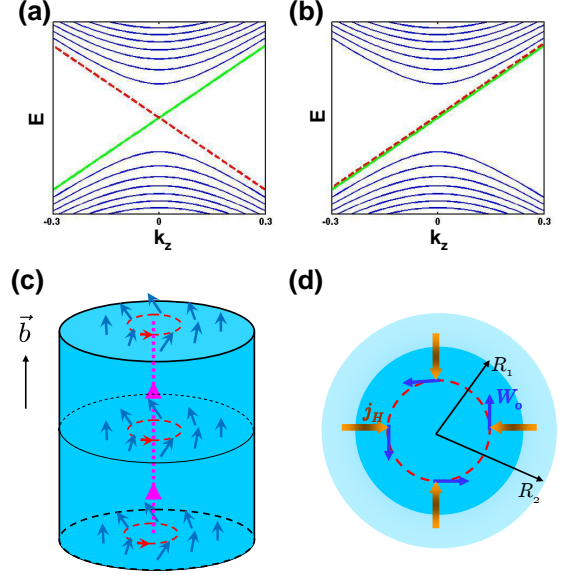


FIG. 1: The Landau level spectrum of a massless Dirac fermion is plotted (a) for a uniform magnetic field \vec{B} and (b) for a uniform “chiral magnetic field” \vec{b} . (c) “Chiral magnetic field” can be generated by the magnetic vortex configuration in a topological insulator cylinder. Here the vector \vec{b} indicates the direction of the “chiral magnetic field”. (d) Top view of the magnetic vortex configuration with the magnetization $W(r) = W_0$ in the regime $r < R_1$ and drop to zero when $r = R_2$.

anomaly equations can be written as

$$\begin{aligned} \partial_\mu j^{\mu 5} &= -\frac{1}{16\pi^2} \epsilon^{\lambda\rho\mu\nu} (F_{\alpha\beta} F_{\mu\nu} + f_{\lambda\rho} f_{\mu\nu}), \quad (2) \\ \partial_\mu j^\mu &= \frac{1}{8\pi^2} \epsilon^{\lambda\rho\mu\nu} f_{\lambda\rho} F_{\mu\nu}. \quad (3) \end{aligned}$$

While equation (2) is the axial current anomaly that has been discussed in the literature^{4,21}, equation (3) indicates that the net charge current also has an anomaly when both chiral gauge field and electromagnetic field are nonzero, which is the main focus of this paper.

Different from the axial current $j^{\mu 5}$, we know that microscopically the net charge current must be conserved without anomaly. However, as we will explain in the following, the anomaly equation (3) is still physically meaningful. As terms in the perturbative expansion of the Hamiltonian, a_μ are always single valued, so that the right side of Eq. (3) can be written in a total derivative $\frac{1}{8\pi^2} \epsilon^{\lambda\rho\mu\nu} f_{\lambda\rho} F_{\mu\nu} = -\partial_\mu j_H^\mu$ with $j_H^\mu = -\frac{1}{2\pi^2} \epsilon^{\mu\nu\lambda\rho} a_\nu \partial_\lambda A_\rho$. Therefore the charge conservation is restored if we view $j_H^\mu + j^\mu$ as the net charge current. Physically, j^μ is the current contributed by the low energy Weyl fermions, while j_H^μ is the “ground state current” carried by the occupied states far away from the fermi surface. This interpretation can be understood more intuitively by a comparison with a 2D quantum Hall state, which has 1D

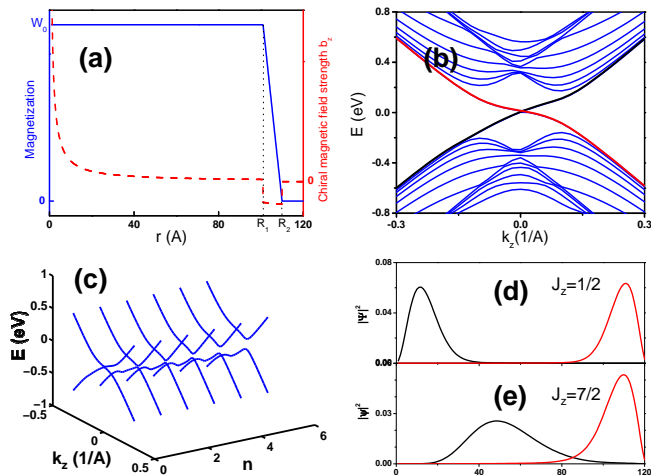


FIG. 2: (a) The radial dependence of chiral vector potential (blue line), and the chiral magnetic field b_z (red line) for a ferromagnetic vortex. (b) The energy dispersion as a function of k_z along a ferromagnetic vortex line with the total angular momentum $J_z = \frac{1}{2}$. The red and black lines indicate the dispersions of two zero modes. (c) The energy dispersion of two zero modes for different $J_z = n + \frac{1}{2}$. The gap observed for large J_z , due to the finite size effect, gives a cut-off of the total number of chiral modes. The radial wave functions for two chiral modes at $k_z = 0$ with total angular momentum (d) $J_z = \frac{1}{2}$ and (e) $J_z = \frac{7}{2}$. Here the black line is for the wave function of the inner chiral mode around $r=0$ and the red line for the one at the outer boundary $r \sim R_{1,2}$. The parameters of the four band model are taken to be $M_0 = 0$, $M_1 = 0.342eV \cdot \text{\AA}^2$, $M_2 = 18.25eV \cdot \text{\AA}^2$, $B_0 = 1.33eV \cdot \text{\AA}$, $A_0 = 2.82eV \cdot \text{\AA}$, $U_0 = 0.1eV$ and $W_0 = 0.06eV$.

chiral edge states. The charge conservation of the edge is broken when an electric field is applied along the edge. From the edge point of view, this is interpreted as the 1D chiral anomaly. From the bulk point of view, this is simply a consequence of the bulk Hall current in the direction perpendicular to the edge. The bulk Hall current is a ground state current, which is contributed by all occupied electrons and cannot be obtained from low energy edge state excitations. The ground state current j_H^μ in our system is an analog of the Hall current in 2D. The correct physical interpretation of the anomaly equation (3) is that the ground state of the Weyl semimetal has a topological response j_H^μ to the external fields a_μ, A_μ , in addition to the current j^μ contributed by low energy excitations near the Weyl points. It should be clarified that although $j^\mu + j_H^\mu$ is conserved, it is generically non-vanished, so that the anomaly equation describes a non-trivial response of the system, as will be seen in the later part of the paper.

III. MICROSCOPIC MODEL

To gain more concrete understanding to the anomaly equations, especially to describe the behavior of the high energy contribution to the current, we would like to go beyond the low energy effective theory approach and consider a microscopic model. In the following we study a microscopic four-band model which describes Weyl fermions and chiral gauge field in magnetically doped topological insulators. By explicit numerical calculation in a magnetic vortex configuration, we demonstrate that the net current in the full microscopic model is consistent with the prediction of anomaly equation.

It has been suggested that Weyl fermions can be realized in pyrochlore iridates¹², HgCr_2Se_4 ¹³, and magnetically doped topological insulators^{14,28}. Pyrochlore iridates and HgCr_2Se_4 have multiple Weyl fermions with the number larger than 2. Minimal number of Weyl fermions can be achieved in magnetically doped Bi_2Se_3 and TlBiSe_2 family of materials, in which ferromagnetism has also been realized²⁹⁻³¹. Here we adopt the four band model^{32,33} with general mass terms, to describe these materials,

$$\begin{aligned}
 H &= H_0 + H_1 & (4) \\
 H_0 &= \epsilon(\vec{k}) + \mathcal{M}(\vec{k})\Gamma_5 + L_1 k_z \Gamma_4 + L_2 (k_y \Gamma_1 - k_x \Gamma_2) \\
 H_1 &= \sum_{ij} m_{ij} \Gamma_{ij}
 \end{aligned}$$

where $\epsilon_{\mathbf{k}} = C_0 + C_1 k_z^2 + C_2 k_{\parallel}^2$, $\mathcal{M}(\mathbf{k}) = M_0 + M_1 k_z^2 + M_2 k_{\parallel}^2$. The Γ matrices are defined as $\Gamma_{1,2,3} = \sigma_{x,y,z} \tau_x$, $\Gamma_4 = \tau_y$, $\Gamma_5 = \tau_z$, and $\Gamma_{ab} = [\Gamma_a, \Gamma_b]/2i$ ($a, b = 1, \dots, 5$). Ferromagnetism breaks \mathbb{T} but preserves \mathbb{P} , therefore by inspecting the symmetry property of Γ matrices (eg. the table III in the reference³³), we immediately find only two sets of Γ matrices are allowed in H_1 : $\Gamma_{ij} = \epsilon_{ijk} \sigma_k$ and $\Gamma_{i4} = \sigma_i \tau_z$ ($i, j, k = x, y, z$). Generally Γ_{12} and Γ_{34} can be induced by z -direction magnetization, while $(\Gamma_{14}, \Gamma_{24})$ and $(\Gamma_{23}, \Gamma_{31})$ originate from in-plane magnetization. It is shown that Γ_{14} , Γ_{24} and Γ_{12} induce two Weyl fermions while Γ_{23} , Γ_{31} and Γ_{34} yield a nodal ring¹⁵. In order to consider the coupling between Weyl fermion and the ferromagnetic fluctuation, we focus on the simple case with $H_1 = U_0 \Gamma_{12}$ with two gap closing points when $|U_0| > |M_0|$, which can be described by Weyl fermions. Then we project the perturbed Hamiltonian $H' = L_1 \delta k_z \tau_y + L_2 (\delta k_y \sigma_x \tau_x - \delta k_x \sigma_y \tau_x) + \sum_{i=x,y,z} (\mu_i \sigma_i + \nu_i \sigma_i \tau_z)$ into the subspace of two Weyl fermions (gap closing points), where $\vec{\mu}$ and $\vec{\nu}$ denote the magnetic fluctuation and $\delta \vec{k}$ is the momentum expanded around gap closing points. Up to the first order for momentum and the second order for magnetic fluctuation, we recover the effective Hamiltonian (1) for the Weyl fermions coupled to a chiral gauge field. The details of microscopic derivation is shown in the appendix.

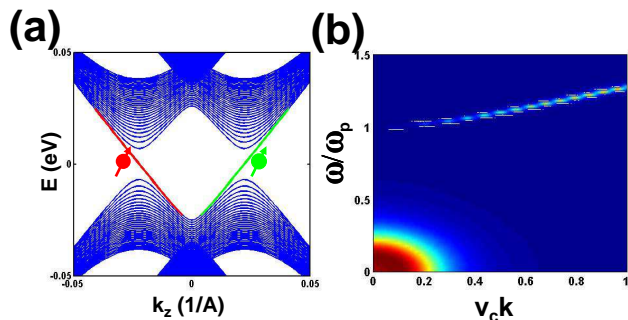


FIG. 3: (a) The Landau levels for the four band model (4) in a uniform magnetic field. (b) The imaginary part of the correlation function $\langle a_z(q)a_z(-q) \rangle$. Here we take $\omega_0/\omega_p = 0.1$, $v_s = 0$.

IV. PHYSICAL CONSEQUENCES OF THE ANOMALY EQUATION

Defining the “chiral magnetic field” $\vec{b} = \nabla \times \vec{a}$ and the “chiral electric field” $\vec{e} = \frac{\partial \vec{a}}{\partial t}$, Eq. (3) can be rewritten as

$$\frac{\partial \rho}{\partial t} + \vec{\nabla} \cdot \vec{j} = \frac{1}{2\pi^2} \left(\vec{b} \cdot \vec{E} + \vec{e} \cdot \vec{B} \right), \quad (5)$$

with ρ and \vec{j} the charge density and current, respectively. In the following we will study the physical consequences of the two terms on the righthand side of this equation.

A. The effect of chiral magnetic field

The first term $\vec{b} \cdot \vec{E}$ describes the effect of a chiral magnetic field parallel to the electric field. To gain some intuition we first consider the Weyl fermion Hamiltonian (1) in a uniform chiral magnetic field $\vec{b} = b_0 \hat{e}_z$. The energy spectrum of this system consists of Landau levels $E_{\pm, \alpha}(n) = \pm \hbar v_f \sqrt{k_z^2 + 2b_0 n}$ with $n = 1, 2, \dots$ and $\alpha = \pm$ denoting two Dirac cones, similar to the Landau levels by a magnetic field. In addition, there are two zeroth Landau levels, both with the dispersion $E_\alpha(0) = -\hbar v_f k_z$ ($\alpha = \pm$), as shown in Fig. 1 (b). It should be noticed that the two zeroth Landau levels are one-dimensional modes with the same velocity (Fig. 1 (b)), in contrast to the opposite velocities for the case of an ordinary magnetic field $\vec{B} = B_0 \hat{e}_z$ shown in Fig. 1 (a). There are two 1D chiral fermion modes per flux quanta of \vec{b} field. In this case, the anomaly equation (5) reduces to the chiral anomaly of 1D chiral fermions^{34,35}.

With the understanding to the consequence of a uniform chiral magnetic field, we now consider a more realistic finite size system described by the four band model (4) with a magnetic vortex configuration shown in Fig. 1 (c). A key difference of the chiral gauge field from the

electromagnetic gauge field is that the gauge vector potential \vec{a} is physical and thus has to be single valued. Therefore the net flux of $\vec{b} = \nabla \times \vec{a}$ must vanish in a finite system (since $\vec{a} = 0$ outside the system). To see the consequence of this effect we consider the magnetic vortex configuration $m_{14} = -W(r) \sin \theta$, $m_{24} = W(r) \cos \theta$, with r the radial coordinate and θ the angular coordinate. $m_{12} = U_0$ and all the other $m_{ij} = 0$. The magnetization amplitude $W(r)$ is a constant W_0 for $r < R_1$ and drops to zero for $r > R_2$, as shown in Fig. 1 (d) and Fig. 2 (a). The corresponding “chiral” magnetic field strength is shown by the red line in Fig. 2 (a), which is positive for $r < R_1$ and negative for $R_1 < r < R_2$. The total flux is zero since there is no magnetization for $r > R_2$. Therefore, the number of chiral modes in region $r < R_1$ is the same as that of anti-chiral modes in region $R_1 < r < R_2$, which is confirmed by our numerical calculation shown in Fig. 2 (b)-(d). The detail of the numerical method is given in the appendix. The energy spectrum can be obtained as a function of the momentum k_z and the angular momentum J_z . The k_z dispersion for states with angular momentum $J_z = 1/2$ is shown in Fig. 2 (b), which contains chiral and anti-chiral modes with spatially localized wave functions shown in Fig. 2 (d). Indeed we see that the chiral and anti-chiral modes are spatially separated. For higher angular momentum J_z , one pair of such chiral and anti-chiral modes exist for each angular momentum but the inner chiral mode moves outwards, as shown in Fig. 2 (e). This is similar to the behavior of Landau level orbits in a uniform magnetic field. For large enough J_z the chiral modes start to overlap with the anti-chiral mode at the boundary region $R_1 < r < R_2$, as shown in Fig. 2 (c). As is expected, the number of chiral modes is determined by the total flux of \vec{a} in region $r < R_1$.

B. The effect of the chiral electric field

In an electric field $\vec{E} = E \hat{z}$ parallel to \vec{b} , the 1D anomaly of the chiral modes describes a charge generation around the center of the system, while the charge on the boundary is annihilated. This is a consequence of the ground state current \vec{j}_H flowing along the radial direction towards the center, as shown in Fig. 1 (d), which can be measured in transport experiments. In other words, the consequence of the anomaly equation (5) in this configuration is equivalent to a quantum Hall effect with Hall current \vec{j}_H ²⁰.

The second term on the right hand side of the anomaly equation (5) describes the combination effect of a magnetic field and a “chiral” electric field. Let’s consider a uniform magnetic field $\vec{B} = B_0 \hat{z}$ and a uniform vector potential $\vec{a} = a_z(t) \hat{z}$ changing adiabatically in time. The anomaly equation leads to $\delta \rho = \frac{G}{2\pi} \delta a_z$, with $G = \frac{e B_0}{h}$ the Landau level degeneracy. Therefore the change of a_z leads to a charge density modulation proportional to it. The Landau level spectrum for the four band model (4) in Fig. 3 (a) possesses two zeroth Landau levels with

the opposite velocities but the same spin polarization. Consequently, the exchange coupling of $\vec{a} = a_z \hat{z}$ with the zeroth Landau level states is equivalent to a scalar potential, which shifts the chemical potential and leads to the change of charge density.

Since this term couples charge density and magnetization, it leads to an interesting physical consequence of the hybridization between the plasmon and magnon modes. Let's consider the Fermi energy is at the two zeroth modes of the Landau levels. Correspondingly, the effective action of this system is given by

$$S_0 = \int \frac{d^2q}{(2\pi)^2} [(A_0(q) + a_z(q))\Pi_{RPA}(A_0(-q) + a_z(-q)) + A_0(q)G_A^{-1}A_0(-q) + a_z(q)G_a^{-1}a_z(-q)] \quad (6)$$

where $q = (\omega, k)$, Π_{RPA} is the RPA correction due to electron-electron interaction and given by $\Pi_{RPA} \sim -\frac{\omega_p^2}{\omega^2}k^2$ in small k limit $k \ll \omega$, $G_A \sim k^{-2}$ is the free photon propagator, and $G_a \sim \frac{1}{q^2 - \omega_0^2}$ is the magnon with the gap ω_0 . We can integrate out A_0 field, leading to

$$S_{eff}^a = \int \frac{d^2q}{(2\pi)^2} a_z(q) \left(G_a^{-1} + \frac{\Pi_{RPA}G_A^{-1}}{\Pi_{RPA} + G_A^{-1}} \right) a_z(-q) \quad (7)$$

Now the second term is given by $-\frac{\omega_p^2 k^2}{\omega^2 - \omega_p^2}$, leading to $G_a^{-1} + \frac{\Pi_{RPA}G_A^{-1}}{\Pi_{RPA} + G_A^{-1}} \sim \omega^2 - k^2 - \omega_0^2 - \frac{\omega_p^2 k^2}{\omega^2 - \omega_p^2}$. We note that when $\omega \sim \omega_p$, the coefficient before k^2 term will diverge, which indicates that a quasiparticle excitation appears at the plasmon frequency for the spin correlation function. In the above expression, we have neglected the velocities, which should be different for light and for spin waves. After recovering the correct velocities, we obtain the spin correlation function given by $\langle a_z(\omega, k)a_z(-\omega, -k) \rangle \sim \left(\omega^2 - v_s^2 k^2 - \omega_0^2 - \frac{\omega_p^2 v_c^2 k^2}{\omega^2 - \omega_p^2 + i0^+} + i0^+ \right)^{-1}$, with magnon velocity v_s , Fermi velocity v_c , plasmon frequency ω_p and magnon excitation gap ω_0 . As plotted in Fig 3 (c), the correlation function has two poles, of which one corresponds to the intrinsic magnon excitation with the frequency around ω_0 , while the other only appears for finite k with the intensity proportional to k^2 and is induced by the plasmons with frequency around ω_p . The plasmon frequency can be estimated as $\sim 35meV$ for Weyl fermions³⁶ with dielectric constant ~ 100 , Fermi velocity $\sim 6.85 \times 10^5 m/s$, and electron density $\sim 10^{19} cm^{-3}$. Such an additional mode in magnon spectrum can be observed in neutron scattering experiments and compared with the plasmon frequency ω_p determined by reflection spectroscopy or electron energy loss spectroscopy.

V. CONCLUSION AND DISCUSSIONS

In conclusion, in this paper we have proposed the realization of chiral gauge field in Weyl semimetals, and

its physical consequences due to axial anomaly. We discussed the general anomaly equations induced by chiral gauge field and electromagnetic gauge field. Based on both low energy effective theory approach and numerical results in a microscopic model of doped topological insulators, we propose two physical consequences of the anomaly, the chiral modes in magnetic vortices, and the magnon-plasmon coupling. An open question is whether it is possible to write down a topological effective field theory to characterize the transport properties of the Weyl semimetals, as in the topological insulators^{5,16,37}. Since there are gapless fermions in Weyl semimetals, it is not clear whether a local bosonic effective field theory can be obtained.

In the end of this paper, we would like to discuss the feasibility of experimental observation of the predicted effects. The main condition for the realization of Weyl semimetal phase is that the exchange coupling due to magnetization is larger than the band gap in the paramagnetic phase. By substituting the atoms, it is possible to tune the band gap of topological insulators, and even induce the phase transition between trivial and non-trivial phases, which has been realized in TlBi(S_{1- δ} Se _{δ})₂³⁸⁻⁴⁰ and Cr doped Bi₂Se₃⁴¹, recently. Near the transition point, the bulk gap is minimized and can be easily overcome by the exchange coupling from magnetic doping. The ferromagnetism in the Cr or Fe doped Bi₂Te₃ and Sb₂Te₃ has been observed in experiment^{29-31,41-44}, therefore the magnetically doped Bi₂Se₃ and TlBiSe₂ family of materials are the suitable platform for the realization of minimal number of Weyl fermions. Different materials are suitable for the two experimental proposals we made. The Cr doped Bi₂Te₃ or Sb₂Te₃^{30,42,43} exhibits ferromagnetism along z-direction, so the topological plasmon-magnon coupling is expected in this system, which can be confirmed by comparing the neutron scattering experiment with reflection spectroscopy or electron energy loss spectroscopy. In another material, Mn doped Bi₂Se₃⁴⁴, it is shown that the magnetization mainly lies in the plane of the film in the ferromagnetic phase. Since the underlying lattice has three-fold rotation symmetry, the ferromagnetic vortex configuration can be realized as the intersection of three 120-degree magnetic domain walls. In general, magnetic vortex configuration can be realized as long as a discrete rotation symmetry C_3, C_4 or C_6 is spontaneously broken. In generic Weyl semimetals, the property of magnetic excitations depends on the material details, such as magnetic structures, material parameters, and it is an interesting direction to understand the interplay between the chiral Weyl fermions and different types of magnetic excitations in realistic materials. Here the disorder effect, such as the scattering between two Weyl fermions, has not been considered. Since Weyl fermion is always gapless, there are always low energy fermionic excitations accompanying the topological contribution to the transport. The interplay between the topological and non-topological contributions to the transport is an interesting question for the future

study.

The authors would like to thank J. Hutasoit, J. Jain, K. Sun, Y.S. Wu, C.K. Xu and S.C. Zhang for helpful discussions. This work is supported by Tsinghua Education Foundation North America (P.Y.), and the Defense Advanced Research Projects Agency Microsystems Technology Office, MesoDynamic Architecture Program (MESO) through the contract number N66001-11-1-4105 (X.L.Q). Research at Perimeter Institute is supported by the Government of Canada through Industry Canada and by the Province of Ontario through the Ministry of Research and Innovation (P.Y.). This work was supported in part by the National Science Foundation under Grant No. NSF PHY11-25915 when the authors participated in the KITP program Topological Insulators and Superconductors. We thank KITP for hospitality.

Appendix A: Microscopic derivation of the effective model for Weyl fermions

In this section of the appendix, we will give a microscopic derivation of the effective model for the coupling between Weyl fermions and magnetic fluctuations. Let's start from the four band Hamiltonian with general mass terms (the equation (4) in the main text). For simplicity, we only consider the case with $m_{12} = U_0$ and other $m_{ij} = 0$. The effective Hamiltonian for this case is given by

$$H_0 + H_1 = \mathcal{M}(\vec{k})\Gamma_5 + L_1 k_z \Gamma_4 + L_2 (k_y \Gamma_1 - k_x \Gamma_2) + m_{12} \Gamma_{12} \quad (\text{A1})$$

where $\mathcal{M}(\mathbf{k}) = M_0 + M_1 k_z^2 + M_2 k_{\parallel}^2$ and ϵ_k term is neglected for simplicity. The energy dispersion of the above Hamiltonian is given by

$$E_{st} = s\sqrt{L_2^2(k_x^2 + k_y^2) + (\sqrt{\mathcal{M}^2 + L_1^2 k_z^2} + t|U_0|)^2} \quad (\text{A2})$$

with $s, t = \pm$. It is clear that for $t = +$, there is always a gap between the branches $|+, +\rangle$ and $|-, +\rangle$. Here we use $|s, t\rangle$ to denote the eigen state with the eigen energy E_{st} . However when $t = -$, the gap between $|+, -\rangle$ and $|-, -\rangle$ can be closed when the condition $\mathcal{M}^2 + B_0^2 k_z^2 = U_0^2$ and $k_x = k_y = 0$ is satisfied. For simplicity, let's neglect the quadratic term in \mathcal{M} first, then it is clear that when $|U_0| > |M_0|$, the above condition is satisfied for some momentum k_z . Therefore, the bulk gap is closed when $|U_0| > |M_0|$ with two closing points given by $k_z = \pm K_0$ and $K_0 = \frac{1}{L_1} \sqrt{U_0^2 - M_0^2}$. Next we need to solve the eigen wave functions at two gap closing points. At $\vec{k} = (0, 0, K_0)$, the eigen equation is written as

$$(M_0 \tau_3 + L_1 K_0 \tau_2 + U_0 \sigma_3) \Phi = E \Phi, \quad (\text{A3})$$

where the quadratic term is neglected. Let's denote the wave function ξ satisfy $(\frac{M_0}{U_0} \tau_3 + \frac{L_1 k_0}{U_0} \tau_2) \xi_\alpha = \alpha \xi_\alpha$, and

$\sigma_3 \chi_\beta = \beta \chi_\beta$, $\alpha, \beta = \pm$, then the corresponding eigen states are given by

$$\begin{aligned} |+, +\rangle &= \chi_+ \otimes \xi_+, & |+, -\rangle &= \chi_- \otimes \xi_+, \\ |-, +\rangle &= \chi_- \otimes \xi_-, & |-, -\rangle &= \chi_+ \otimes \xi_- \end{aligned} \quad (\text{A4})$$

with ξ and χ given by

$$\begin{aligned} \xi_+ &= \frac{1}{\sqrt{N_+}} \begin{pmatrix} iL_1 K_0 \\ M_0 - U_0 \end{pmatrix}, & \xi_- &= \frac{1}{\sqrt{N_-}} \begin{pmatrix} iL_1 K_0 \\ M_0 + U_0 \end{pmatrix}, \\ \chi_+ &= \begin{pmatrix} 1 \\ 0 \end{pmatrix}, & \chi_- &= \begin{pmatrix} 0 \\ 1 \end{pmatrix} \end{aligned} \quad (\text{A5})$$

where N_{\pm} are the normalization factors and we assume $U_0 > 0$ for simplicity. Now we consider the effective Hamiltonian expanded around $(0, 0, K_0)$,

$$\begin{aligned} H' &= L_1 \delta k_z \tau_y + L_2 (\delta k_y \sigma_x \tau_x - \delta k_x \sigma_y \tau_x) \\ &+ \sum_{i=x,y,z} (\mu_i \sigma_i + \nu_i \sigma_i \tau_z), \end{aligned} \quad (\text{A6})$$

and project it into the subspace spanned by the basis $|-, -\rangle$ and $|+, -\rangle$ with the second order perturbation

$$\begin{aligned} H_{mn} &= \langle m | H_1 | n \rangle + \\ &\sum_{l \neq m, n} \frac{1}{2} \langle m | H_1 | l \rangle \langle l | H_1 | n \rangle \left[\frac{1}{E_m - E_l} + \frac{1}{E_n - E_l} \right] \end{aligned} \quad (\text{A7})$$

which leads to the following Hamiltonian

$$\begin{aligned} H_{eff}^{(1)} &= -\frac{M_0}{U_0} v_z - \left(\frac{L_1^2 K_0}{U_0} \delta k_z - u_z \right) \sigma_z + \\ &\left(-L_2 \delta k_x + \frac{L_1 K_0}{U_0} v_x \right) \sigma_x + \left(-L_2 \delta k_y + \frac{L_1 K_0}{U_0} v_y \right) \sigma_y \end{aligned} \quad (\text{A8})$$

for the first order perturbation and

$$\begin{aligned} H_{eff}^{(2)} &= -\frac{M_0}{U_0^2} (u_x v_x + v_y u_y) - \\ &\frac{1}{2U_0} \left(v_z^2 - u_x^2 - u_y^2 - \frac{M_0^2}{U_0^2} \sum_i v_i^2 \right) \sigma_z \\ &- \frac{L_1 K_0}{U_0^2} v_z u_x \sigma_x - \frac{L_1 K_0}{U_0^2} v_z u_y \sigma_y \end{aligned} \quad (\text{A9})$$

for the second order perturbation. Here we only keep the momentum term up to the first order and \vec{u} , \vec{v} terms up to the second order. If we only look at the momentum term, then clearly this just provides the Weyl fermion in three dimensions. For the expansion near $(0, 0, -K_0)$ point, we can perform similar calculation and obtain

$$\begin{aligned} H_{eff}^{(1)} &= -\frac{M_0}{U_0} v_z - \left(-\frac{L_1^2 K_0}{U_0} \delta k_z - u_z \right) \sigma_z + \\ &\left(L_2 \delta k_x + \frac{L_1 K_0}{U_0} v_x \right) \sigma_x + \left(L_2 \delta k_y + \frac{L_1 K_0}{U_0} v_y \right) \sigma_y \end{aligned} \quad (\text{A10})$$

for the first order perturbation and

$$\begin{aligned}
H_{eff}^{(2)} &= -\frac{M_0}{U_0^2} (u_x v_x + v_y u_y) \\
&- \frac{1}{2U_0} \left(v_z^2 - u_x^2 - u_y^2 - \frac{M_0^2}{U_0^2} \sum_i v_i^2 \right) \sigma_z \\
&- \frac{L_1 K_0}{U_0^2} v_z u_x \sigma_x - \frac{L_1 K_0}{U_0^2} v_z u_y \sigma_y
\end{aligned} \quad (A11)$$

for the second order perturbation. Therefore eventually our effective low energy Hamiltonian for the system takes the form

$$\begin{aligned}
H_{eff} &= \hbar v_{fz} (\delta k_z \sigma_z \tau_z + a_z \sigma_z) + \\
\hbar v_{f\parallel} &\sum_{i=x,y} (\delta k_i \sigma_i \tau_z + a_i \sigma_i)
\end{aligned} \quad (A12)$$

where σ denotes spin, τ represents two Dirac cones at $(0, 0, \pm K_0)$, the Fermi velocity $\hbar v_{fz} = -\frac{L_1^2 K_0}{U_0}$, $\hbar v_{f\parallel} = -L_2$ and the chiral gauge potential \vec{a} is given by

$$\hbar v_{fz} a_z = \mu_z - \frac{1}{U_0} \left(\nu_z^2 - \mu_x^2 - \mu_y^2 - \frac{M_0^2}{U_0^2} \sum_i \nu_i^2 \right) \quad (A13)$$

$$\hbar v_{f\parallel} a_x = \frac{L_1 K_0}{U_0} \nu_x - \frac{L_1 K_0}{U_0^2} \nu_z \mu_x \quad (A14)$$

$$\hbar v_{f\parallel} a_y = \frac{L_1 K_0}{U_0} \nu_y - \frac{L_1 K_0}{U_0^2} \nu_z \mu_y. \quad (A15)$$

Therefore, the perturbation from ferromagnetic fluctuation can only shift the position of the touching point of a single Weyl fermion, behaving like a gauge field. Furthermore, the ferromagnetic type of coupling breaks time reversal but preserves parity, therefore it can not be conventional gauge field like the electromagnetic field. So finally the only choice is chiral gauge field.

Appendix B: Numerical method for the calculation of the chiral mode in the ferromagnetic vortex core

In the section of the appendix, we describe our numerical method for the calculation of energy dispersion and

eigen wavefunction for the ferromagnetic vortex configuration. We start from the four band model (4) in the main text and in the cylinder coordinate (r, θ, z) , the Hamiltonian takes the form of

$$H = H_0 + H_1 \quad (B1)$$

$$H_0 = \mathcal{M}(\vec{k}) \tau_z + L_1 k_z \tau_y + L_2 (k_y \sigma_x \tau_x - k_x \sigma_y \tau_x)$$

$$= \begin{pmatrix} \mathcal{M}(\vec{k}) & 0 & -iL_1 k_z & iL_2 k_- \\ 0 & \mathcal{M}(\vec{k}) & -iL_2 k_+ & -iL_1 k_z \\ iL_1 k_z & iL_2 k_- & -\mathcal{M}(\vec{k}) & 0 \\ -iL_2 k_+ & iL_1 k_z & 0 & -\mathcal{M}(\vec{k}) \end{pmatrix}$$

$$H_1 = -W_0 \sin \theta \sigma_x \tau_z + W_0 \cos \theta \sigma_y \tau_z + U_0 \sigma_z$$

$$= \begin{pmatrix} U_0 & -iW_0 e^{-i\theta} & 0 & 0 \\ iW_0 e^{i\theta} & -U_0 & 0 & 0 \\ 0 & 0 & U_0 & iW_0 e^{-i\theta} \\ 0 & 0 & -iW_0 e^{i\theta} & -U_0 \end{pmatrix}$$

where we have $\partial_x = \cos \theta \partial_r - \frac{\sin \theta}{r} \partial_\theta$ and $\partial_y = \sin \theta \partial_r + \frac{\cos \theta}{r} \partial_\theta$, therefore $k_- = k_x - ik_y = -i\partial_x - \partial_y = -i(\cos \theta \partial_r - \frac{\sin \theta}{r} \partial_\theta) - (\sin \theta \partial_r + \frac{\cos \theta}{r} \partial_\theta) = -ie^{-i\theta} \partial_r - \frac{e^{-i\theta}}{r} \partial_\theta$, $k_+ = -i\partial_x + \partial_y = -i(\cos \theta \partial_r - \frac{\sin \theta}{r} \partial_\theta) + (\sin \theta \partial_r + \frac{\cos \theta}{r} \partial_\theta) = -ie^{i\theta} \partial_r + \frac{e^{i\theta}}{r} \partial_\theta$ and $k_x^2 + k_y^2 = -\left(\frac{\partial^2}{\partial r^2} + \frac{1}{r} \frac{\partial}{\partial r} + \frac{1}{r^2} \frac{\partial}{\partial \theta^2}\right)$. The above Hamiltonian has in-plane rotation symmetry along z axis and the corresponding total angular momentum can be defined as $J_z = L_z + \frac{1}{2} \sigma_z$ where $L_z = -i\frac{\partial}{\partial \theta}$ and the Pauli matrix σ_z denotes the spin part. With the in-plane rotation symmetry, the wavefunction ansatz can be taken as $\tilde{\psi}(r, \theta) = [e^{in\theta} f_1(r), e^{i(n+1)\theta} f_2(r), e^{in\theta} f_3(r), e^{i(n+1)\theta} f_4(r)]^T$ where the total angular momentum $J_z = n + \frac{1}{2}$. The Hamiltonian is changed to

$$\tilde{H} = \begin{pmatrix} \tilde{\mathcal{M}}(n) + U_0 & -iW_0 & -iL_1 k_z & L_2 \left(\partial_r + \frac{n+1}{r}\right) \\ iW_0 & \tilde{\mathcal{M}}(n+1) - U_0 & L_2 \left(-\partial_r + \frac{n}{r}\right) & -iL_1 k_z \\ iL_1 k_z & L_2 \left(\partial_r + \frac{n+1}{r}\right) & -\tilde{\mathcal{M}}(n) + U_0 & iW_0 \\ L_2 \left(-\partial_r + \frac{n}{r}\right) & iL_1 k_z & -iW_0 & -\tilde{\mathcal{M}}(n+1) - U_0 \end{pmatrix} \quad (B2)$$

where $\tilde{\mathcal{M}}(n) = M_0 + M_1 k_z^2 - M_2 \left(\frac{\partial^2}{\partial r^2} + \frac{1}{r} \frac{\partial}{\partial r} - \frac{n^2}{r^2}\right)$ and the wave function is now given by $\tilde{\psi} = [f_1(r), f_2(r), f_3(r), f_4(r)]^T$. Let's introduce the new wave

function ψ as $\tilde{\psi} = \frac{1}{\sqrt{r}} \psi$, then the normalization relation $\int r dr d\theta |\tilde{\psi}|^2 = 1$ is changed to $\int dr d\theta |\psi|^2 = 1$, and the effective Hamiltonian is rewritten as

$$H = \begin{pmatrix} \mathcal{M}(n) + U_0 & -iW_0 & -iL_1k_z & L_2 \left(\partial_r + \frac{n+1/2}{r} \right) \\ iW_0 & \mathcal{M}(n+1) - U_0 & L_2 \left(-\partial_r + \frac{n+1/2}{r} \right) & -iL_1k_z \\ iL_1k_z & L_2 \left(\partial_r + \frac{n+1/2}{r} \right) & -\mathcal{M}(n) + U_0 & iW_0 \\ L_2 \left(-\partial_r + \frac{n+1/2}{r} \right) & iL_1k_z & -iW_0 & -\mathcal{M}(n+1) - U_0 \end{pmatrix} \quad (\text{B3})$$

where $\mathcal{M}(n) = M_0 + M_1k_z^2 - M_2 \left(\frac{\partial^2}{\partial r^2} - \frac{n^2-1/4}{r^2} \right)$. This Hamiltonian can be written in a compact form

$$H = \left[M_0 + M_1k_z^2 - M_2 \left(\frac{\partial^2}{\partial r^2} - \frac{(n+1/2)^2}{r^2} \right) \right] \tau_z - M_2 \frac{n+1/2}{r^2} \sigma_z \tau_z + L_1k_z \tau_y + iL_2 \frac{\partial}{\partial r} \sigma_y \tau_x + L_2 \frac{n+1/2}{r} \sigma_x \tau_x + W_0 \sigma_y \tau_z + U_0 \sigma_z. \quad (\text{B4})$$

We can discretize the Hamiltonian (B3) and solve the eigenstate problem for the radial equation numerically. The corresponding result is shown in Fig 2 of the main text. For $n = 0$, we indeed find two gapless modes with the opposite velocities along z direction, and these two gapless modes are spatially separated with one wave function mainly staying at $r = 0$ and the other one at $r = R$, as shown by the red and black lines in Fig 2 (b) and (d) of the main text. However with increasing n , a gap is opened between the two low energy modes, as shown in Fig 2 (c) in the main text. To get more analytical understanding of the radial equation, we consider the $r \rightarrow \infty$ limit with $U_0 = 0$, $k_z = 0$, where the radial Hamiltonian is simplified as $H = \left(M_0 - M_2 \frac{\partial^2}{\partial r^2} \right) \tau_z + W_0 \sigma_y \tau_z + iL_2 \sigma_y \tau_x \frac{\partial}{\partial r}$. With the wave function ansatz $\psi \sim e^{\lambda r} \phi$, we obtain the equation $L_2 \lambda \phi = \left[(M_0 - M_2 \lambda^2) \sigma_y \tau_y + W_0 \tau_y \right] \phi$ for the zero modes. Since $[\sigma_y \tau_y, \tau_y] = 0$, we can take the common eigen-states of $\sigma_y \tau_y$ and τ_y for ϕ , $\sigma_y \tau_y \phi_{ts} = t \phi_{ts}$ and $\tau_y \phi_{ts} = s \phi_{ts}$, then the wave function can be expressed as $\psi = \sum_{\alpha, t, s} c_{\alpha, ts} e^{\lambda_{\alpha}(t, s) r} \phi_{t, s}$, with λ given by $\lambda_{\alpha}(t, s) = \frac{-tL_2 + \alpha \sqrt{L_2^2 + 4M_2(tsW_0 + M_0)}}{2M_2}$. The existence of the edge mode requires $\lambda_+(+, +)\lambda_-(-, +) > 0$ or $\lambda_+(+, -)\lambda_-(-, -) > 0$, leading to the following different regimes: in the normal regime $M_0M_2 > 0$, the system has no zero mode when $|W_0| < |M_0|$ and one zero mode when $|W_0| > |M_0|$, while in the inverted regime $M_0M_2 < 0$, the system has one zero mode when $|W_0| > |M_0|$ and two zero modes when $|W_0| < |M_0|$. Taking into account the k_z dependent term, it turns out that one zero mode case corresponds to the 1D chiral state and two zero modes case is the 1D helical state. However since time reversal is broken in the present system, the helical state is not

protected and can be gapped. Therefore the only robust state is the chiral state when $|W_0| > |M_0|$. We emphasize that the transition at $|W_0| = |M_0|$ exactly corresponds to the condition for the appearance of the gapless Weyl fermions for the uniform magnetization. For the finite r , the terms proportional to $\frac{1}{r}$ and $\frac{1}{r^2}$ will push the chiral mode around $r=0$ outwards, thus with increasing the angular momentum number n , the wave function of the chiral mode near $r = 0$ extends to the large r region and mixes with the chiral mode at $r = R$, opening a gap.

-
- ¹ M. E. Peskin and D. V. Schroeder, *An Introduction to Quantum Field Theory* (Addison-Wesley Publishing Company, Massachusetts, 1995).
- ² S. L. Adler, *Phys. Rev.* **177**, 2426 (1969).
- ³ J. Bell and R. Jackiw, *Nuovo Cimento A* **60**, 47 (1969).
- ⁴ H. Nielsen and M. Ninomiya, *Physics Letters B* **130**, 389 (1983).
- ⁵ X.-L. Qi, T. L. Hughes, and S.-C. Zhang, *Phys. Rev. B* **78**, 195424 (2008).
- ⁶ D. B. Kaplan, *Physics Letters B* **288**, 342 (1992), ISSN 0370-2693.
- ⁷ C. G. Callan and J. A. Harvey, *Nucl. Phys. B* **250**, 427 (1985).
- ⁸ X.-L. Qi and S.-C. Zhang, *Rev. Mod. Phys.* **83**, 1057 (2011).
- ⁹ M. Z. Hasan and C. L. Kane, *Rev. Mod. Phys.* **82**, 3045 (2010).
- ¹⁰ J. E. Moore, *Nature* **464**, 194 (2009).
- ¹¹ G. Volovik, *The Universe in a Helium Droplet* (Clarendon Press, Oxford, 2003).
- ¹² X. Wan, A. M. Turner, A. Vishwanath, and S. Y. Savrasov, *Phys. Rev. B* **83**, 205101 (2011).
- ¹³ G. Xu, H. Weng, Z. Wang, X. Dai, and Z. Fang, *Phys. Rev. Lett.* **107**, 186806 (2011).
- ¹⁴ A. A. Burkov and L. Balents, *Phys. Rev. Lett.* **107**, 127205 (2011).
- ¹⁵ A. A. Burkov, M. D. Hook, and L. Balents, *Phys. Rev. B* **84**, 235126 (2011).
- ¹⁶ G. Y. Cho and J. E. Moore, *Annals of Physics* **326**, 1515 (2011).
- ¹⁷ C. Fang, M. J. Gilbert, X. Dai, and B. A. Bernevig, e-print arxiv:1111.7309 (2011).
- ¹⁸ J. Jiang, e-print arxiv:1112.5943 (2011).
- ¹⁹ P. Hosur, S. A. Parameswaran, and A. Vishwanath, *Phys. Rev. Lett.* **108**, 046602 (2012).
- ²⁰ K.-Y. Yang, Y.-M. Lu, and Y. Ran, *Phys. Rev. B* **84**, 075129 (2011).
- ²¹ V. Aji, e-print arxiv:1108.4426 (2011).
- ²² H. B. Nielsen and M. Ninomiya, *Nucl. Phys. B* **193**, 173 (1981).
- ²³ H. B. Nielsen and M. Ninomiya, *Nucl. Phys. B* **185**, 20 (1981).
- ²⁴ A. H. Castro Neto, F. Guinea, N. M. R. Peres, K. S. Novoselov, and A. K. Geim, *Rev. Mod. Phys.* **81**, 109 (2009).
- ²⁵ K. K. Gomes, W. Mar, W. Ko, F. Guinea, and H. C. Manoharan, *Nature* **483**, 306 (2012).
- ²⁶ A. Zee, *Quantum Field Theory in a Nutshell* (Princeton University Press, New Jersey, 2010).
- ²⁷ K. Fujikawa and H. Suzuki, *Path integrals and quantum anomalies* (Oxford, Clarendon, UK, 2004).
- ²⁸ G. Y. Cho, e-print arXiv:1110.1939 (2011).
- ²⁹ Y. L. Chen, J. H. Chu, J. G. Analytis, Z. K. Liu, K. Igarashi, H. H. Kuo, X. L. Qi, S. K. Mo, R. G. Moore, D. H. Lu, et al., *Science* **329**, 659 (2010).
- ³⁰ C. Chang, J. Zhang, M. Liu, Z. Zhang, X. Feng, K. Li, L. Wang, X. Chen, X. Dai, Z. Fang, et al., e-print arXiv:1108.4754 (2011).
- ³¹ L. A. Wray, S. Xu, Y. Xia, D. Hsieh, A. V. Fedorov, Y. S. Hor, R. J. Cava, A. Bansil, H. Lin, and M. Z. Hasan, *Nat Phys* pp. 32–37 (2011).
- ³² H. Zhang, C. Liu, X. Qi, X. Dai, Z. Fang, and S. Zhang, *Nat Phys* **5**, 438 (2009).
- ³³ C.-X. Liu, X.-L. Qi, H.-J. Zhang, X. Dai, Z. Fang, and S.-C. Zhang, *Phys. Rev. B* **82**, 045122 (2010).
- ³⁴ K. Johnson, *Physics Letters* **5**, 253 (1963).
- ³⁵ R. Jackiw, *Topological investigations of quantized gauge theories*, in *Current Algebra and Anomalies*, edited by Sam B. Treiman, Roman Jackiw, Bruno Zumino and Edward Witten, Princeton University Press, 1985.
- ³⁶ S. Das Sarma and E. H. Hwang, *Phys. Rev. Lett.* **102**, 206412 (2009).
- ³⁷ A. Chan, T. L. Hughes, S. Ryu, and E. Fradkin, *Phys. Rev. B* **87**, 085132 (2013).
- ³⁸ B. Yan, C. Liu, H. Zhang, C. Yam, X. Qi, T. Frauenheim, and S. Zhang, *EPL (Europhysics Letters)* **90**, 37002 (2010).
- ³⁹ H. Lin, R. S. Markiewicz, L. A. Wray, L. Fu, M. Z. Hasan, and A. Bansil, *Phys. Rev. Lett.* **105**, 036404 (2010).
- ⁴⁰ S. Xu, Y. Xia, L. A. Wray, S. Jia, F. Meier, J. H. Dil, J. Osterwalder, B. Slomski, A. Bansil, H. Lin, et al., *Science* **332**, 560 (2011).
- ⁴¹ J. Zhang, C.-Z. Chang, P. Tang, Z. Zhang, X. Feng, K. Li, L.-l. Wang, X. Chen, C. Liu, W. Duan, et al., *Science* **339**, 1582 (2013).
- ⁴² C.-Z. Chang, J. Zhang, M. Liu, Z. Zhang, X. Feng, K. Li, L.-L. Wang, X. Chen, X. Dai, Z. Fang, et al., *Advanced Materials* **25**, 1065 (2013), ISSN 1521-4095.
- ⁴³ M. Liu, J. Zhang, C.-Z. Chang, Z. Zhang, X. Feng, K. Li, K. He, L.-l. Wang, X. Chen, X. Dai, et al., *Phys. Rev. Lett.* **108**, 036805 (2012).
- ⁴⁴ D. Zhang, A. Richardella, D. W. Rench, S.-Y. Xu, A. Kandala, T. C. Flanagan, H. Beidenkopf, A. L. Yeats, B. B. Buckley, P. V. Klimov, et al., *Phys. Rev. B* **86**, 205127 (2012).